Handbook of Clinical Neurology, Vol. 160 (3rd series)
Clinical Neurophysiology: Basis and Technical Aspects
K.H. Levin and P. Chauvel, Editors
https://doi.org/10.1016/B978-0-444-64032-1.00012-6

Chapter 12

High-resolution EEG

CHRISTOPH M. MICHEL*
Department of Basic Neurosciences, University of Geneva, Geneva, Switzerland
Center for Biomedical Imaging (CIBM) Lausanne-Geneva, Geneva, Switzerland

Abstract

High-resolution EEG recording has become standard in many experimental studies on human brain function and has found its place in the routine presurgical workup of patients with focal epilepsy in several clinical centers. The main aim of high-resolution EEG is source localization with methods that have become increasingly robust and precise. However, high-resolution EEG also allows a spatial analysis of EEG and evoked potentials on the scalp level, thereby identifying topographic features of the scalp potential field. Their value in understanding the dynamics of large-scale networks of the human brain and as markers for neuropsychiatric diseases has been increasingly demonstrated. This chapter discusses the advantages and limitations of such spatial analysis methods and the information that can be gained from them. It also shows that the spatial frequency of the scalp potential field is higher than previously assumed and discusses the consequences regarding the number of channels required to properly capture these spatial frequencies.

INTRODUCTION

Recording an electroencephalogram (EEG) from multichannel arrays has become increasingly popular due to advances in hardware and software technology. The number of publications using the term "high-density EEG" in the title or keywords has increased 10-fold during the last 20 years. Very quickly after the discovery of EEG, it became apparent that EEG signals vary substantially over the scalp (Adrian and Matthews, 1934) and that signals from different scalp areas should be recorded routinely in clinical practice, leading to distributed electrode placement (e.g., the 10–20 electrode placement (Jasper, 1958)).

Intuitively, one would assume that more electrodes placed on the scalp would correspond to richer information derived from these signals. This sentiment has been weakened by simultaneous intracranial and scalp recordings that suggested that several (6–10) square centimeters of cortex need to be active to generate a signal on the scalp (Cooper et al., 1965), so dense electrode spacing would simply oversample the electric field generated by such large patches of activity. However, this size estimation, which was based on epileptic activity, has been repeatedly shown to be incorrect. According to calculations reviewed in Hämälainen et al. (1993), only 40–200 mm^2 of cortical surface must be simultaneously active to produce a nonnegligible extracranial field. Therefore, depending on the event being recorded, the spatial frequency of the scalp potential field can be much higher so that low-density recordings lead to spatial aliasing, mislocalization, and loss of focal signals. EEG-arrays with interelectrode distances of less than 2 cm were recommended by many authors, leading to 100–200 electrodes if the whole head surface is to be covered.

Such high-density recordings inevitably lead to the question of how to analyze these multiple signals properly, given that they are neither spatially nor temporally independent. Terms such as brain mapping, EEG field mapping, or brain topography have been introduced by

*Corresponding author: Professor Christoph M. Michel Ph.D., Functional Brain Mapping Laboratory, Department of Basic Neurosciences, Campus Biotech 9, chemin des Mines, Geneva, 1202, Switzerland. Tel: +41-22-379-54-57, E-mail: christoph.michel@unige.ch

researchers looking at such multichannel recordings (Ragot and Remond, 1978; Nunez, 1981; Duffy, 1986; Lehmann, 1987; Maurer, 1989; Gevins et al., 1990; Wong, 1990). These terms refer to the analysis of the spatial distribution of the potential field on the scalp that is generated through volume conduction from the active neuronal populations in the brain. Since changes in the topography of these potential fields or maps are due to changes in the distribution of the active neuronal populations in the brain (Vaughan, 1982) by physical law, a common approach in the analysis of multichannel EEG is to describe and compare EEG maps in different conditions. Characterizing the topographies of evoked potential components, epileptic spikes, powers in certain frequency bands, or certain characteristic oscillations, such as spindles or slow waves, has become a common approach in many high-density EEG studies. EEG topographic maps are the precursors for source localization (Fender, 1987), and the configuration of these maps can provide (if properly interpreted) an initial clue for the possible localization of the underlying sources. If the maps statistically differ over time, between conditions, or between clinical populations, then the conclusion that different brain networks were active is valid (Lehmann et al., 1987). However, proper statistical pattern recognition methods are required to distinguish map configurations. Importantly, however, the inverse is not true: similar map configurations do not permit the conclusion that the same generators were active in the brain. Many different configurations of simultaneously active sources can lead to the same topography of the potential field on the scalp. This is the so-called "inverse problem" (Helmholtz, 1853).

This chapter discusses the need for high-resolution EEG and describes and illustrates different methods of topographic analysis for EEG and evoked potentials. It discusses the information that can be gained from such analysis compared to classic waveform analyses and the advantages and limitations of the interpretation of the results derived from them.

SPATIAL ANALYSIS OF EEG

Sampling from distributed electrode arrays can reveal the topographic distribution of the potential field in terms of potential maps. Therefore, the amplitude at each electrode site is represented as a color, and amplitudes at unmeasured sites are interpolated to present a smooth color display on a stylized picture of the head. Such mapping techniques were promoted heavily in the late 1970s and early 1980s as a tool to easily localize the areas of altered brain function in neurological and psychiatric diseases, leading to considerable commercial activities (John et al., 1977; Duffy, 1985). This initial enthusiasm has been hampered by demonstrations of misinterpretation of these maps and by evidence showing that it adds very little to the visual analysis of the EEG by competent electroencephalographers (Harner, 1988; Nuwer, 1990; Duffy et al., 1994; Nuwer, 1997).

The overinterpretation of the localization of brain functions based on the visual inspection of brain maps led to considerable discrediting of the method. Nevertheless, these initial efforts to focus on the spatial distribution of the potential field on the scalp triggered a growing interest in quantitative spatial analysis methods, ultimately leading to source imaging techniques for which EEG brain maps are the precursor (Fender, 1987). Currently, source localization based on high-resolution EEG has become standard in many experimental and clinical studies, and methods to select the spatial features that may be used to localize alterations in brain functions have become available (Michel and Murray, 2012). The spatial analysis of multichannel EEG has matured from the initial qualitative description of colored brain maps to a powerful quantitative brain imaging technique.

Reference independence of EEG maps

Traditionally, EEG and evoked potentials are analyzed by characterizing waveform features such as the amplitude and frequency of a spontaneous EEG, peak latency, or the polarity and amplitude of evoked potential components. Since EEG is a bipolar signal by definition, these features depend on the choice of the recording reference. The recorded signal at a given electrode always reflects the local activity at the target and at the reference site. This fact is well-known by clinical electrophysiologists, who naturally look at EEG signals with different derivation schemes in routine clinical EEG. By doing so, electrophysiologists enhance the appreciation of the spatial distribution of the signal of interest. EEG mapping has the same purpose: it visualizes the spatial distribution of a given electrophysiologic event. Importantly, the topography of the EEG map is reference-independent. The reference only changes the zero-level (DC-shift), but the topographical features of the map remain unaffected (Lehmann, 1987; Pascual-Marqui and Lehmann, 1993; Geselowitz, 1998). Therefore, the topographic analysis of the EEG is reference-free and eliminates the reference problem of the EEG (Lehmann, 1987). The same holds for EEG source imaging, which is entirely based on the spatial distribution of the electric field and is also not affected by the position of the reference as long as the reference electrode is placed on the scalp and is included in the topographic reconstruction of the potential field (Pascual-Marqui et al., 2009).

While the reference-independence of EEG and evoked potential maps is an important advantage of EEG mapping analyses as compared to waveform analyses, it is important to note that this does not hold for data transformed in the frequency domain: frequency transformation using FFT or time–frequency analysis calculates the amplitude and phase of a signal at a given electrode with respect to the reference electrode. Changing the reference electrode changes both the amplitude and the phase at the target location and consequently changes the topographic distribution of the power at a given frequency (Lehmann et al., 1986). Therefore, topographic analysis in the time-domain is reference-free, but topographic analysis in the frequency-domain is not (Lehmann, 1987). Fig. 12.1 illustrates this important fact, which has significant consequences for frequency-domain analyses of EEG, including the increasingly used analysis of functional connectivity between EEG sensors.

Chella et al. (2016) recently demonstrated the impact of the reference on such analysis by showing significant reference-dependent differences in EEG functional connectivity and graph network properties on the scalp level. The same authors also showed how the reference choice influences bispectral analyses (Chella et al., 2017). Similar problems have been noted in studies on the hemispheric asymmetry of cortical activity in given frequency bands, where Hagemann et al. (2001) illustrated how asymmetry of the frontal alpha power depends on the selected reference scheme.

Global map descriptors

A well-established descriptor of the global strength of the electric field recorded at a given moment in time is the global field power (GFP) (Lehmann and Skrandies, 1980; Michel et al., 1993). Global field power is the

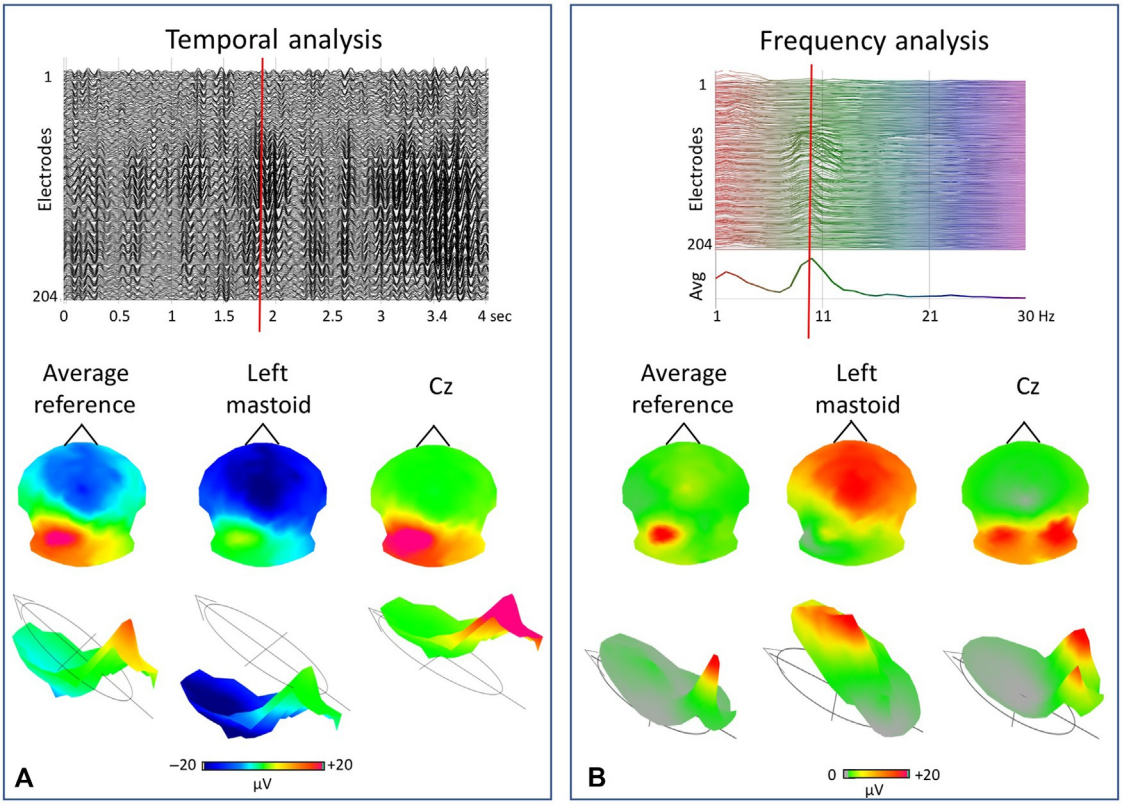

Fig. 12.1. Effect of the reference electrode on scalp potential maps. (A) Four seconds of eyes-closed spontaneous EEG, filtered in the alpha band. 2D scalp potential maps (seen from *top*, nose *up*, left ear *left*) are shown for a selected time point below, referenced to three different references (average reference, left mastoid, Cz). On the *bottom*, the same maps are shown as 3D surface plots with elevations proportional to the potential values. Obviously, changing the reference only changes the zero-level of the map (indicated with the zero plane) but does not change the topography (the landscape) of the map. (B) Frequency analysis of the same EEG with an FFT over a 2-s time window. The spectrum for each electrode and the average power are shown on *top*. The power maps as well as the 3D surface plots at 10 Hz are shown *below* when the FFT is computed with the same three different reference settings as in (A). In this case, changing the reference obviously changes the topography of the power maps, with maximal power appearing at different electrodes.

standard deviation of the potentials at all electrodes of an average-reference map. It is defined as

$$\mathrm{GFP} = \sqrt{\sum_{i=1}^{N} (u_1 - \bar{u})^2 \Big/ N} \qquad (12.1)$$

where u_i is the voltage of the map u at electrode i, $\bar{u}$ is the average voltage of all electrodes of map u (the average reference) and N is the number of electrodes in map u. Scalp potential fields with prominent positive and negative peaks, or very "hilly" maps, will result in high GFP, but "flat" maps with shallow gradients display low GFP. Calculating the GFP over time allows the identification of moments with high signal-to-noise ratios, presumably corresponding to moments of high global neuronal synchronization (Skrandies, 1990).

To compare the topography between two maps independent of field strength, Lehmann and Skrandies (1980) introduced the calculation of the global map dissimilarity (GMD). The reference-independent measure is defined as

$$\mathrm{GMD} = \sqrt{\frac{1}{N}\sum_{i=1}^{N} \left\{ \frac{u_i - \bar{u}}{\sqrt{\sum_{i=1}^{N} \frac{(u_i - \bar{u})^2}{N}}} - \frac{v_i - \bar{v}}{\sqrt{\sum_{i=1}^{N} \frac{(v_i - \bar{v})^2}{N}}} \right\}^2} \qquad (12.2)$$

where u_i is the voltage of map u at electrode i, v_i is the voltage of map v at electrode i, $\bar{u}$ is the average voltage of all electrodes of map u (the average reference), $\bar{v}$ is the average voltage of all electrodes in map v, and N is the total number of electrodes. Since only topography is of interest rather than strength differences, the two maps that are compared are first normalized by dividing the potential values at each electrode of a given map by its GFP, which is indicated in the denominator of Eq. (12.2).

The GMD is 0 when two maps are equal and maximally reaches 2 if the two maps have the same topography with reversed polarity. GMD is equivalent to the spatial Pearson's product–moment correlation coefficient between the potentials of the two maps ($\mathrm{GMD}^2 = 2 * (1 - r)$; Brandeis et al., 1992).

As discussed previously, if two maps differ in topography independently of their strengths, this directly indicates that the two maps were generated by different configurations of sources in the brain (Fender, 1987; Michel et al., 2004b). Therefore, the GMD calculation is the first step for defining whether different sources were involved in the two maps that were compared. When calculating the GMD between two subsequent maps, one notes that the GMD inversely correlates with the GFP: GMD is high when GFP is low and vice versa. This interesting observation indicates that maps tend to have stable topographies during periods of high GFP and change their configuration when GFP is low (Fig. 12.2); that is, maps do not continuously change configurations over time.

The GMD itself is not a statistical measure. It only gives a spatial correlation value. However, the GMD can be used as a parameter to statistically compare map topographies between groups or experimental conditions. This is achieved by performing nonparametric randomization tests based on the GMD values (Murray et al., 2008), called the topographic analysis of variance (tANOVA). A tANOVA is conducted in the following way: (1) assign the maps of a single subject to different experimental conditions or groups in a randomized fashion (i.e., permutations of the data); (2) calculate the average EEG map for the permuted groups or conditions and the GMD between them; and (3) compare the GMD values from the actual groups or conditions with the values from the distribution of the randomly shuffled data to determine the likelihood that the empirical data has a value higher than the GMD from the shuffled distribution. An analysis of variance with multiple factors can also be performed in this way (Koenig and Melie-Garcia, 2010).

Spatiotemporal decomposition of multichannel EEG

EEG provides redundant information because the signals are highly correlated both in time and in space, which leads to a challenge for statistical analysis methods that consider each electrode and each time point. Conventional correction methods for multiple testing are inappropriate for highly correlated signals. Global topographic parameters, such as the GFP and the GMD, reduce this problem by representing one-numbered reference-free topographic descriptors for each time point. Therefore, they allow the reduction of the data in time by only considering the time points with the highest signal-to-noise ratios (GFP peaks) or by averaging the data between subsequent GMD peaks, since the topography remains stable in between (Michel et al., 1992; Skrandies, 1993; Fig. 12.2).

The redundancy of time-varying, multichannel EEG data led researchers to propose spatiotemporal decomposition methods to find a series of distinct components or modes that describe the signal and ultimately find distinct components that differ between experimental or clinical conditions. Traditionally, such decomposition is carried out in the frequency domain by spectral analyses of the EEG and computing the power spectrum, thereby assuming quasistationarity of the signal (Lopes da Silva and Mars, 1987). Transient oscillations are decomposed by estimating the time-varying spectrum using wavelet analysis techniques (Bertrand et al., 1994; Basar et al., 1999).

Because such analysis is usually performed on individual channels, the topographic distribution is

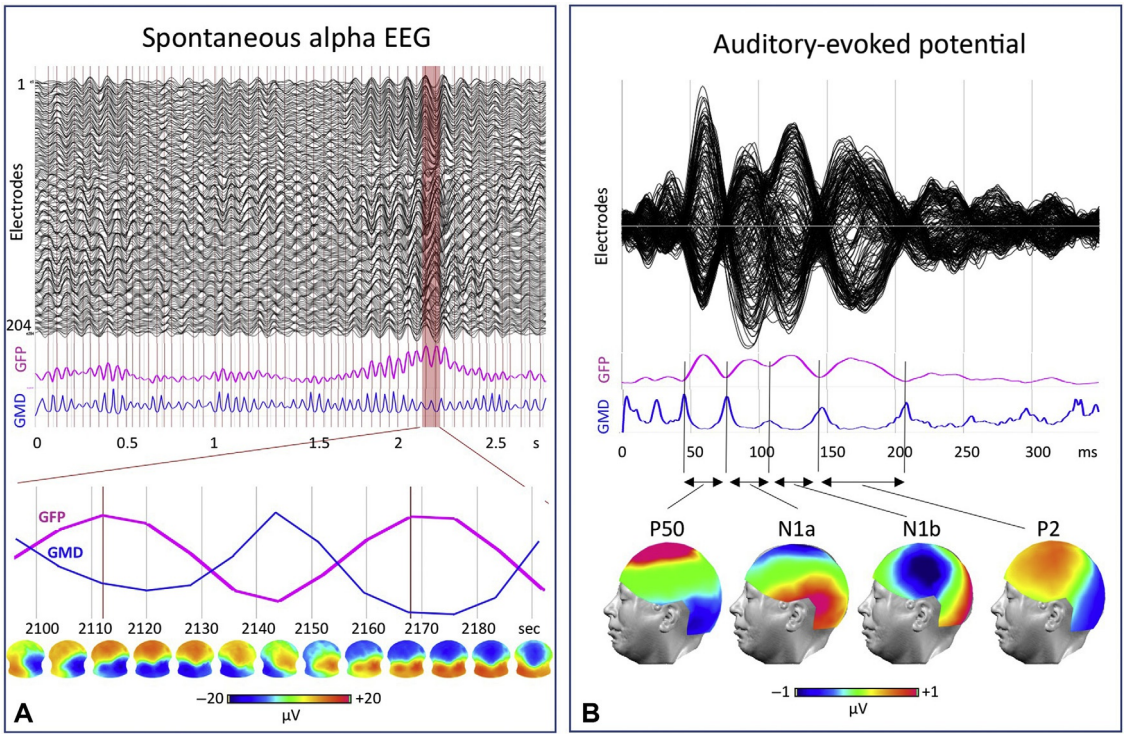

Fig. 12.2. Global map descriptors. The two global map descriptors global field power (GFP) and global map dissimilarity (GMD) are illustrated as time courses in spontaneous EEG (A) and evoked potentials (B). Both cases show that GFP and GMD exhibit opposite behavior over time: GMD is low when GFP is high and vice versa, indicating that maps tend to be stable in topography when the field is strong and change the topography during weak fields. In (A), maps at each time point over two successive GFP peaks are shown. In (B), maps are averaged between two GMD peaks, revealing the well-known topographies of the auditory evoked potentials. Both the selection of maps at the GFP peaks in the spontaneous EEG and the averaging of maps between two GMD peaks in evoked potentials have been used for data reduction and component definition (see text).

often ignored, implicitly assuming that the spatial configuration of the neural sources that generate the component remains stable. A simple inspection of the topographies of a frequency-filtered multichannel EEG clarifies that this is not the case (Fig. 12.3): this figure shows that the topography of the scalp potential map of the alpha-filtered EEG changes over time, indicating that different neural sources contributed to the alpha signal on the scalp at different points in time. Consequently, the decomposition of multichannel EEG should consider the time-varying spatial configuration of the electric field, whether in the time or the frequency domain.

Most commonly, spatial factor analysis methods are used to decompose multichannel EEG into distinct components, represented as maps. These maps represent the weighted sum of all recorded channels across time and the load for each of these factors varies in time. The most commonly used spatial decompositions are based on principal component analysis (PCA) and independent component analysis (ICA) (Harner, 1988; Skrandies, 1989; Koles et al., 1995; Makeig et al., 1997; Hyvarinen and Oja, 2000; Jung et al., 2001; Dien et al., 2005).

The PCA imposes orthogonality between different factors. The first component of PCA accounts for the maximally possible amount of data variance and each subsequent orthogonal component accounts for the maximum possible residual variance. PCA has been proven to be a powerful exploratory tool to extract those components in multichannel event-related potentials that differ between experimental conditions (Kayser and Tenke, 2005; Pourtois et al., 2008).

Instead of orthogonality, the ICA imposes statistical independence. Each factor is supposed to represent a temporally independent component. Like the PCA, the ICA produces a weight coefficient for each factor. The ICA has been proven to be very useful for the detection and removal of artifacts such as eye-blinks (Jung et al., 2000) or artifacts produced by brain-independent sources such as the ballistocardiogram artifact of an EEG recorded in an MRI scanner (Benar et al., 2003; Nakamura et al., 2006; Mantini et al., 2007; Debener et al., 2008). The ICA has also been used to decompose brain activity into independent brain processes (Makeig et al., 1997, 1999). However, the assumption of the statistical independence of brain processes is challenged by the fact that crosstalk between brain regions and within

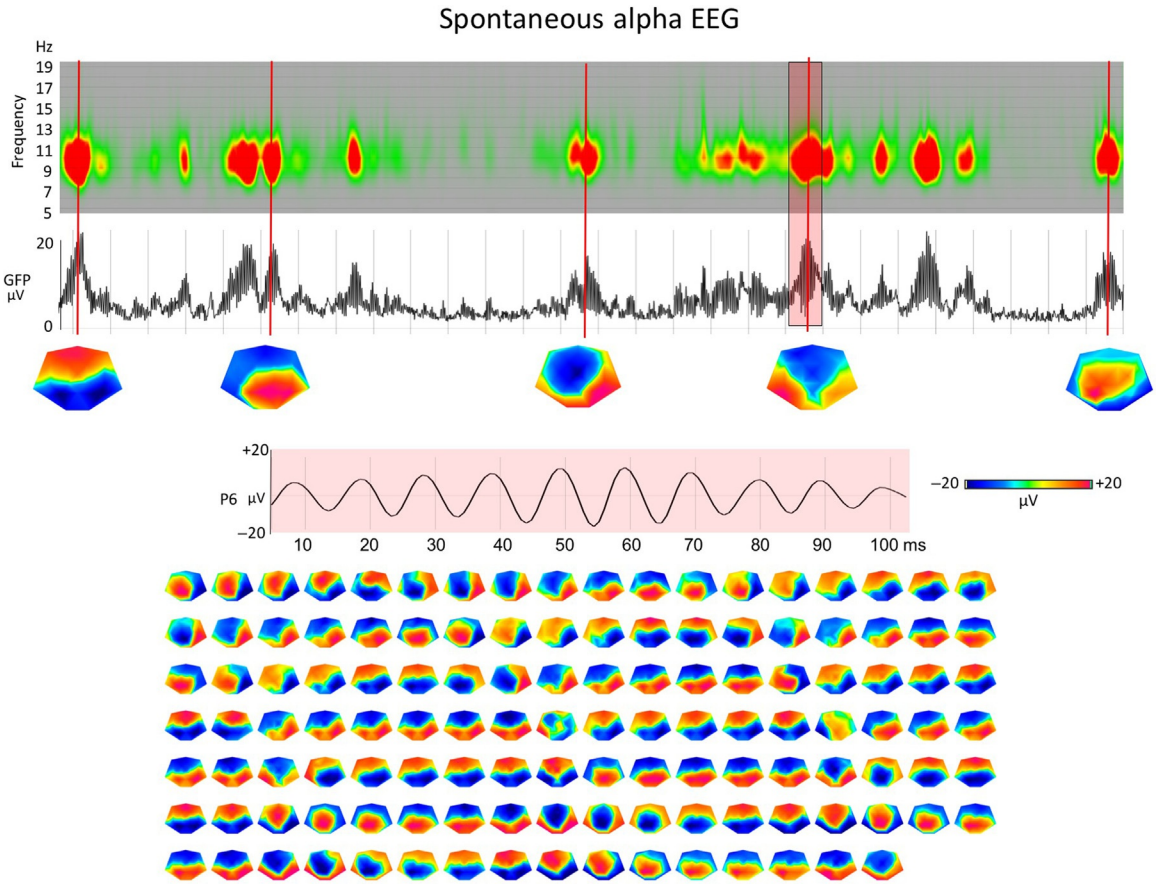

Fig. 12.3. Spatial nonstationarity of alpha-EEG. The analysis of EEG in a certain frequency band, for example using power-envelope analysis, assumes that the generators of this activity remain stable in time and only change their activity strength. This figure illustrates that this assumption is not valid: the top shows the wavelet analysis of an eyes-closed EEG. The power is averaged over all channels, showing typical alpha bursts at different time periods. *Below*, the GFP of the EEG is shown and maps at peaks of alpha activity are plotted. Obviously, the topography of the maps at different time points are very different, indicating a different distribution of alpha generators in the brain. On the *bottom* a period of 100-ms EEG during one alpha burst is shown (marked in *red* on the EEG) and the maps at each time point are plotted. This example shows that, even during an alpha burst, map topographies change, indicating changes in the underlying generators also during these short intervals.

distributed neural networks is certainly one of the main principles of brain organization (Womelsdorf et al., 2007). Therefore, the main limitation of the ICA is that it cannot uncover components that are dynamically coupled.

A widely used method to determine the spatial components of EEG and event-related potentials is based on spatial *k*-means clustering, a method that is generally used in pattern-recognition applications. In a modified version of *k*-means clustering, Pascual-Marqui et al. (1995) suggested the use of the GMD parameter described previously (Eq. 12.2) to cluster maps with high spatial correlations and determine the centroid of these clusters as a representative template map for each cluster. Cross-validation and other criteria are used to determine the optimal number of clusters (Pascual-Marqui et al., 1995; Murray et al., 2009; Brunet et al., 2011; Custo et al., 2017).

The *k*-means clustering technique does not assume statistical independence or orthogonality of the maps. In a nested iterative way, it defines the best number of clusters to optimally explain the data with a minimal number of maps. Interestingly, when fitting these cluster maps back to the data, it appears that one specific map often dominates for a certain amount of time (some 100 ms), whether in spontaneous EEG or in event-related potential data. It has been suggested that these periods of stable topography represent states of global phase-locked synchronized activity in large-scale neuronal networks (Koenig et al., 2005). In event-related potentials, these epochs may represent different steps of information processing (Brandeis and Lehmann, 1986), but in spontaneous EEG, these "EEG microstates" may represent the basic building blocks of mentation, or the "atoms of thought" (Lehmann et al., 1987; for reviews, see Lehmann, 1990;

Lehmann et al., 2009; Lehmann and Michel, 2011; Michel and Koenig, 2017; Fig. 12.4).

Many different studies have shown that the configuration, duration, presence, and transition probabilities of the microstates are influenced by stimulus parameters, the global state of the brain, and the consciousness level, and that they are disturbed in different neurological and psychiatric diseases (for reviews, see Khanna et al., 2015; Rieger et al., 2016; Michel and Koenig, 2017).

In conclusion, spatiotemporal decomposition methods using ICA, PCA, or *k*-means clustering each have intrinsic advantages and limitations. What they have in common is that they try to separate the different sources that comprise the multichannel scalp recordings, i.e., to separate the different temporally independent networks that are active over time. Even if these methods do not directly specify the location in the brain where these activations are coming from, they provide a useful preprocessing step for source localization (Jung et al., 2001).

Source localization

Even before the promotion of brain mapping as a tool to visualize the spatial distribution of the electric field and eventually localize the origins of the recorded scalp signals, it has been recognized that the basic electric field theory can be used to relate the electric potential differences on the scalp to a current dipole in the brain (Geisler and Gerstein, 1961). These equations were used in 1969 to localize the generator of a visual evoked potential (Lehmann et al., 1969). Single dipole localization procedures have subsequently become popular and were the subject of several experimental and clinical studies in the 1980s (Ary et al., 1981; Darcey and Williamson, 1985; Fender, 1987).

A major improvement was introduced by Scherg and von Cramon that involved spatiotemporal dipole modeling for the localization of several dipoles with varying strengths over time (Scherg and von Cramon, 1985), an idea that was subsequently extended by the MUSIC approach (Mosher et al., 1992). Commercial software tools became available using this approach, leading to the increased use of this method in the EEG (particularly in evoked potentials) community (Scherg et al., 1989; Scherg and Picton, 1991). Some reasonable results have been produced using these dipole fitting approaches, particularly with respect to the localization of epileptic foci and early evoked potential components (Scherg and Ebersole, 1994; Picton et al., 1999; Di Russo et al., 2005; Waberski et al., 2008; Rose and Ebersole, 2009). However, the assumptions and constraints imposed by this method are very strong and physiologically unreasonable in many cases in which multiple simultaneously active sources with different locations, strengths, and orientations must be assumed. Consequently, more reasonable approaches for source localization have been developed over the last 30–40 years by many different research groups (for review, see Michel et al., 2004b; Pascual-Marqui et al., 2009; Salmelin and Baillet, 2009; Michel and He, 2018; He and Ding, 2013).

Currently, most source localization studies use distributed source modeling approaches that estimate the current density distribution in the whole brain based on scalp recordings. Initiated by the seminal papers of Hämäläinen and Ilmoniemi (1984) and Hämälainen et al. (1993) that introduced the minimal norm approach, new algorithms based on this initial idea of a linearly distributed inverse solution were developed that further enhanced localization precision.

The most commonly used algorithms were LORETA and its derivates (Pascual-Marqui et al., 1994; Pascual-Marqui, 2002), FOCUSS (Gorodnitsky et al., 1995), VARETA (Bosch-Bayard et al., 2001), LAURA (Grave de Peralta Menendez et al., 2004), and beamforming approaches (Sekihara et al., 2001). The details of these approaches and the underlying constraints are discussed in Chapter 8.

Basically, this family of techniques consists of a linear system of equations that relate the known part of the system (the measurements at each electrode) to the unknowns (the current density vectors at discrete points throughout the cortical gray matter, i.e., the "solution space"). At each solution point, a current density vector (i.e., a dipole) is placed. The coefficients of the linear system of equations correspond to the lead field, which relates the extracranial measurements to a source by the laws of electrodynamics (distance, geometry, and conductivity profile). The set of coefficients is highly underdetermined, because there are many more solution points than measurable recording channels, known as the nonuniqueness of the inverse problem.

Many different configurations and orientations of sources at the different solution points can lead to the same scalp electric field. Therefore, physiologically and biophysically meaningful constraints must be incorporated. This is where the different algorithms vary. For example, although the initially introduced minimal norm solution only minimizes the least-square error of the estimated inverse solution, LORETA minimizes the second spatial derivative so that the estimation is smooth.

Many experimental studies in very different fields have shown that these methods allow the localization of the sources in the cortex that generated the scalp recordings in an impressively reliable way (He and Lian, 2002, 2005; Michel et al., 2004b, 2009; Sanei and Chambers, 2007; He et al., 2011b; Michel and Murray, 2012; He and Ding, 2013). By adding realistic individual head models with appropriate conductivity

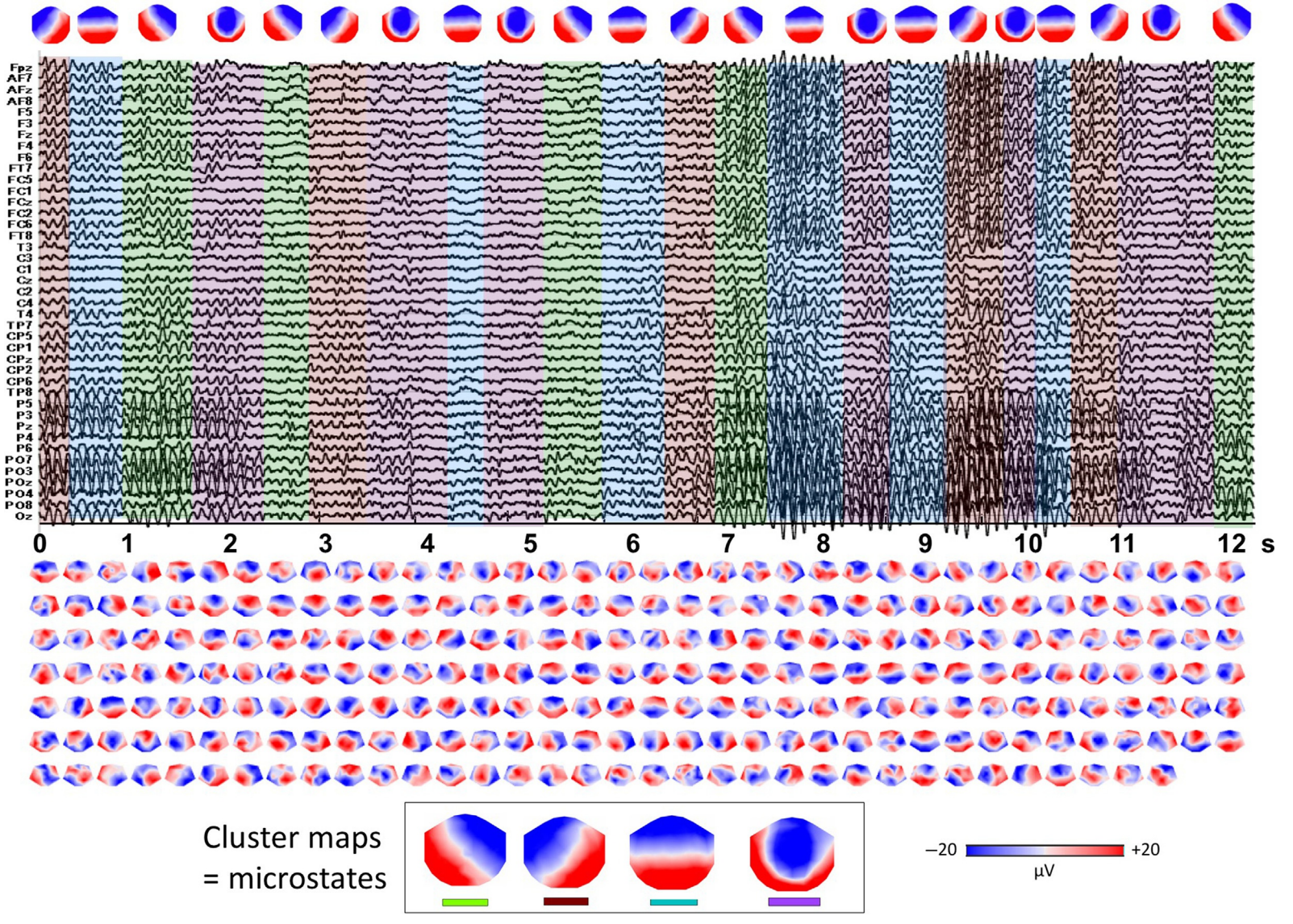

Fig. 12.4. EEG segmentation into microstates. A 12-s eyes-closed EEG recorded from 41 electrodes is shown together with the sequence of potential maps (shown every 50 ms). The map series was subjected to a *k*-means cluster analysis, revealing the four classic maps described in the literature (see text). These maps were then fitted to the EEG data by means of spatial correlation using the GMD measure and each time point was labeled with the map it correlated with best by a winner-takes-all strategy. The fitting leads to periods during which a given map is dominant, lasting in average around 100 ms, the so-called microstate. The duration, occurrence, and temporal succession of the maps have been shown to be sensitive parameters for different levels of consciousness and different neuropsychiatric diseases. For a recent review see Michel and Koenig (2017).

parameters, the localization precision for cortical sources has been shown to be in the range of approximately 15 mm (Birot et al., 2014; Lascano et al., 2014; Megevand et al., 2014; Klamer et al., 2015). Most crucial, however, are the number and the distribution of the electrodes that are used to record the electric field, a point that will be discussed in the following section.

HIGH-RESOLUTION EEG: HOW MANY ELECTRODES ARE NEEDED?

The question of how many electrodes are needed for a proper spatial analysis of the EEG has been asked since the beginning of the promotion of EEG mapping techniques. In a critical paper on EEG brain mapping published by Richard Harner in 1988, he asked the crucial question: "How widespread are EEG fields, both normal and abnormal, over the head? What is their spatial frequency, that is, how many field peaks (spatial waves) need to be represented per meter? How numerous and how closely spaced need electrodes be on the head in order to represent fields of a given distribution and a given spatial frequency? These questions have rarely been addressed rigorously by electroencephalographers but are essential for signal analysis in the spatial domain, just as the corresponding questions have been accepted as essential for analysis in the time or frequency domains" (Harner, 1988, p. 74).

Meanwhile, this question has been addressed in several studies. It basically relates to the question of the maximal spatial frequency of the scalp potential field. Similar to the analysis of time series, the Nyquist theorem also applies to the analysis of scalp potential maps: the highest spatial frequency that can properly be analyzed depends on the sampling of the signal. If the signal is undersampled, (spatial) aliasing will occur (Li and North, 1996). This means that if the spatial sampling frequency (i.e., the distance between electrodes) is lower than the spatial frequencies of the potential field, the reconstructed map topography will be distorted, leading to misinterpretation of the maps and mislocalization of the sources (Srinivasan et al., 1996, 1998; Grieve et al., 2004; Ryynanen et al., 2004; Ryynanen et al., 2006). Therefore, knowledge of the maximal spatial frequency of the scalp electric field is important and has been repeatedly discussed over the years.

Initial studies based on simulations (Gevins et al., 1990) and experimental data (Spitzer et al., 1989) indicated that an interelectrode distance of ~2–3 cm is needed, which would lead to approximately 100 electrodes required for whole coverage of the scalp. Based on spatial spectral density estimations, Freeman et al. (2003) concluded that even less than 1-cm spacing of electrodes is required. Srinivasan et al. (1998) compared the effective spatial resolution of different electrode montages (19–129 electrodes) and concluded that "the smallest topographic feature that can be resolved accurately by a 32-channel array is 7 cm in diameter, or about the size of a lobe of the brain." These authors also compared the scalp topography of the visually evoked N1 component between 129 electrodes and fewer electrodes and showed that fewer electrodes led to incorrect lateralization and the appearance of a fronto-central positive focus.

Other studies calculated the potential maps of simulated single dipoles and then estimated the dipole location using source localization techniques with different numbers of scalp electrodes (Lantz et al., 2003; Michel et al., 2004b; Sohrabpour et al., 2015). These studies showed increasing source localization precision with an increasing number of electrodes, reaching a plateau at approximately 100 electrodes. They also showed that increasing the number of electrodes reduces the localization error of deep sources.

Several experimental studies evaluated the effect of electrode number on source localization precision by using only subsamples of the originally recorded electrodes. Michel et al. (2004b) showed that the visual P100 component is incorrectly lateralized when only 19 of the available 46 electrodes were used. They also showed that incomplete coverage of the head can lead to misplacement of the estimated sources. Luu et al. (2001) studied patients with acute focal ischemic stroke. They were initially recorded using 128 electrodes and then subsampled to 64, 32, and 19 channels. By visually comparing the EEG maps with radiographic images, the authors conclude that more than 64 electrodes were needed to avoid mislocalizations of the affected regions. Lantz et al. (2003) recorded epileptic spikes from 14 patients with focal epilepsy with 123 electrodes and then subsampled them to 63 and 31 electrodes. Source localization was then applied to the individual spikes with the different electrode arrays and the localization maximum was compared to the resected zone that rendered the patients seizure-free. Source localization accuracy systematically increased from 31 to 123 electrodes.

A more recent study of Sohrabpour et al. (2015) used the same method in a pediatric population of epileptic patients and evaluated the localization error by comparing the source localization with the seizure onset zone defined by intracranial recordings. They also found a systematic increase in localization precision by increasing the number of electrodes from 32 to 64 and to 128.

The most comprehensive study on localization of the irritative zone using high-resolution EEG was published by Brodbeck et al. (2011). In a prospective study on 152 operated patients, they evaluated the clinical yield of the EEG source imaging of interictal spikes. They showed a

sensitivity of 84% and a specificity of 88% for EEG source imaging if the EEG was recorded with a large number of electrodes (128–256 channels) and when using the individual MRI as a head model in the source reconstruction. These values drastically decreased when EEG source imaging was performed with only 32-channel recordings and even more so when a template head model was used.

Most simulation and experimental studies described here estimated that approximately 100 electrodes are needed for correct spatial sampling of the electric field. However, most of these studies assumed that the skull-scalp ratio of the resistance is 80:1, as assumed many years ago by Rush and Driscoll (1969). Several recent studies have shown that the skull resistance is considerably lower, in the range of 20:1 (Oostendorp et al., 2000; Hoekema et al., 2003; Lai et al., 2005). The skull resistance has an important effect on the spatial resolution of the EEG by drastically blurring the signals (Malmivuo and Suihko, 2004). Ryynanen et al. (2004) systematically investigated the benefit of a higher number of electrodes on spatial resolution when lowering the resistance values. They first showed that the typically used high resistance ratio of 80:1 indeed leads to a limited spatial resolution that can be correctly captured with approximately 64 electrodes. Then, they reduced the skull resistance and showed that continuously increasing the number of electrodes above 64 improves the spatial resolution.

The resistance of the skull depends on skull thickness. It has been shown that the skull thickness is approximately 7–8 times lower in infants compared to adults, leading to a ratio of approximately 14:1 (Grieve et al., 2004; Fifer et al., 2006) between the skull and the brain. Ryynanen et al. (2006) and Grieve et al. (2004) showed that with this ratio, spatial resolution still increases with 256 compared to 128 electrodes. Therefore, in contrast to the intuitive assumption that the smaller heads of infants require fewer electrodes, the thinner skull warranted more electrodes than in adults to reduce the spatial sampling error, particularly in neonates (Odabaee et al., 2013, 2014).

Since the spatial frequency of the EEG is higher than previously assumed, the size of a cortical area responsible for producing a measurable EEG signal needs to be reconsidered. The density of active neurons and the degree of correlation among them are important factors. If focal cortical activity can be captured by the EEG, such activities can be missed with low-density electrode arrays. A recent study by Zelmann et al. (2014) nicely illustrated this fact. With simulations and with simultaneous scalp and intracranial recordings, the authors showed that high-frequency oscillations (HFOs; frequency range 80–500 Hz) can be recorded on the scalp despite their low amplitudes and their very focal generators, but they can be easily missed if no electrode is placed above such focal generators (Fig. 12.5).

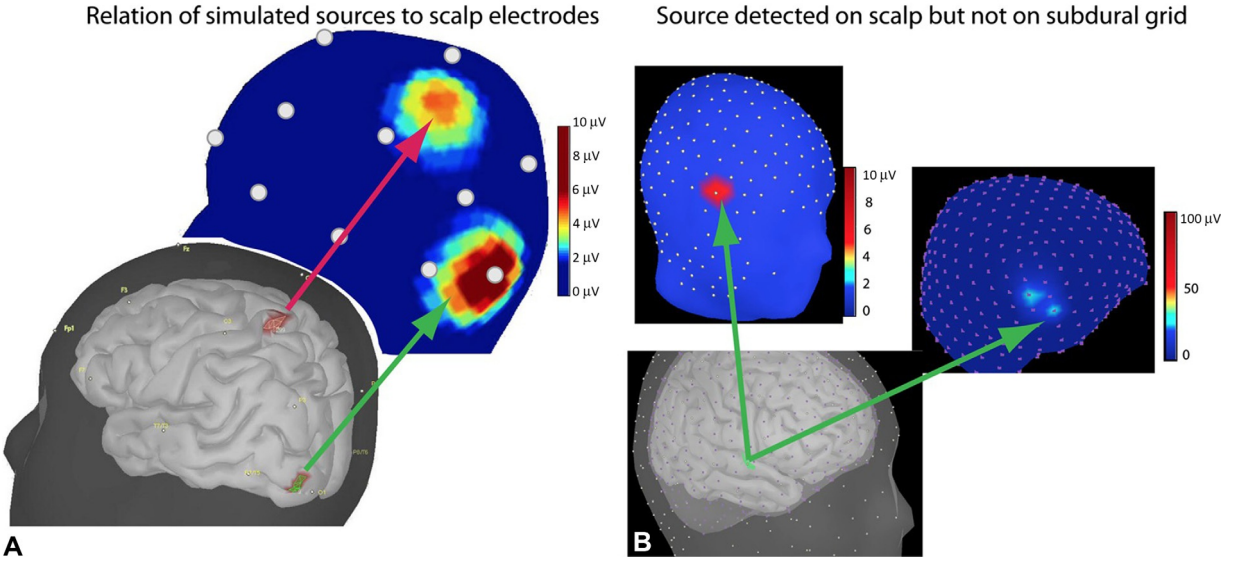

Fig. 12.5. Detection of high-frequency oscillations (HFOs) with high-resolution EEG. In a simulation study, Zelmann et al. illustrate the scalp distribution of focal sources as produced by HFOs. (A) When EEG is recorded with electrodes according to the 10–20 system, only one of the sources (*green*) is captured, while the other source (*magenta*) is missed. (B) Recordings of a 256-channel scalp EEG is compared with a recording from a subdural grid with 1.3-cm separation between contacts. The subdural grid would miss the focal source that falls between two contacts, while the scalp EEG would capture it by an electrode above the source. From Zelmann R, Lina JM, Schulze-Bonhage A et al. (2014). Scalp EEG is not a blur: it can see high frequency oscillations although their generators are small. Brain Topogr 27: 683–704.

To illustrate this fact, Zelmann et al. (2014) simulated distributed sources of approximately 1 cm^2 in size and showed that only 14% of these small sources were visible on the scalp with the 10–20 system, 38% with the 10–10 system, and 71% with 256 electrodes. Therefore, electrophysiologic events of such small spatial extent can only be detected by proper sampling of the electric field (see also Kuhnke et al., 2018).

Lu et al. (2014) confirmed the detection of focal HFO sources with high-density EEG and further demonstrated that they can be correctly localized with source imaging methods. These studies also clearly show that there is no specific filtering of high frequencies by the skull, as sometimes erroneously stated in textbooks. The conductivity of the skull remains the same from 1 Hz to 10 kHz (Oostendorp et al., 2000; Tang et al., 2008). Zelmann et al. (2014) also noted that another reason for the detection of HFOs despite their low amplitudes is that their frequencies are beyond the frequencies that generate the noise in the signal and thus have favorable signal-to-noise ratios.

Recently, Petrov et al. (2014) argued for an even higher number of electrodes. They demonstrated in an event-related potential study that a spatial sampling of the EEG with a 1-cm interelectrode distance (corresponding to around 760 electrodes) revealed almost twice the amount of functional brain signals as compared to sampling at 3-cm scale (corresponding to approximately 100 electrodes). However, the technology for such ultradense EEG arrays has yet to be developed.

In addition to the need for sufficient electrodes to correctly capture the spatial frequencies of the electric field and avoid spatial aliasing and missing focal sources, the electric field must be sampled as completely as possible (Fig. 12.6). Neuronal activity in the brain spreads homogeneously in all directions to the scalp, leading to

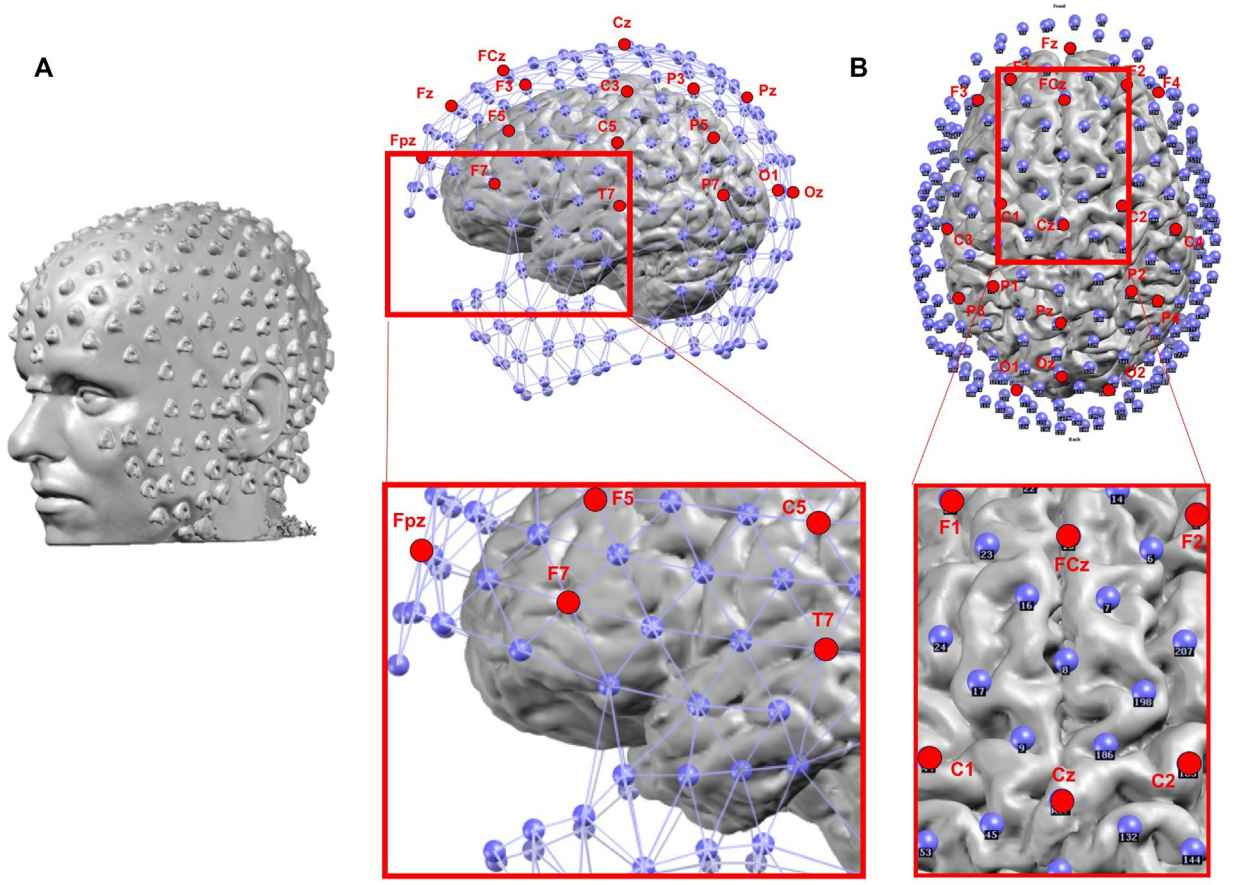

Fig. 12.6. Illustration of spatial sampling and spatial coverage. A subject was placed with a 256-channel EEG (Geodesics, Inc.) in an MR scanner. (A) The reconstructed image of the head shows the position of the electrodes as artifacts in the MR images. (B) The extracted brain shows the position of the electrodes in relation to the brain surface. The electrodes corresponding to the 10–20 system are marked in *red*. The zoomed enlargements show that the 10–20 system does not cover a large part of the temporal pole and fronto-orbital cortex, making it impossible to record activities generated in these areas. Also, the sparse sampling makes it impossible to distinguish the hemisphere in sources close to the interhemispheric fissure, an example of which is shown in Fig. 12.7 for the foot motor area. Courtesy: Dr. Laurent Spinelli.

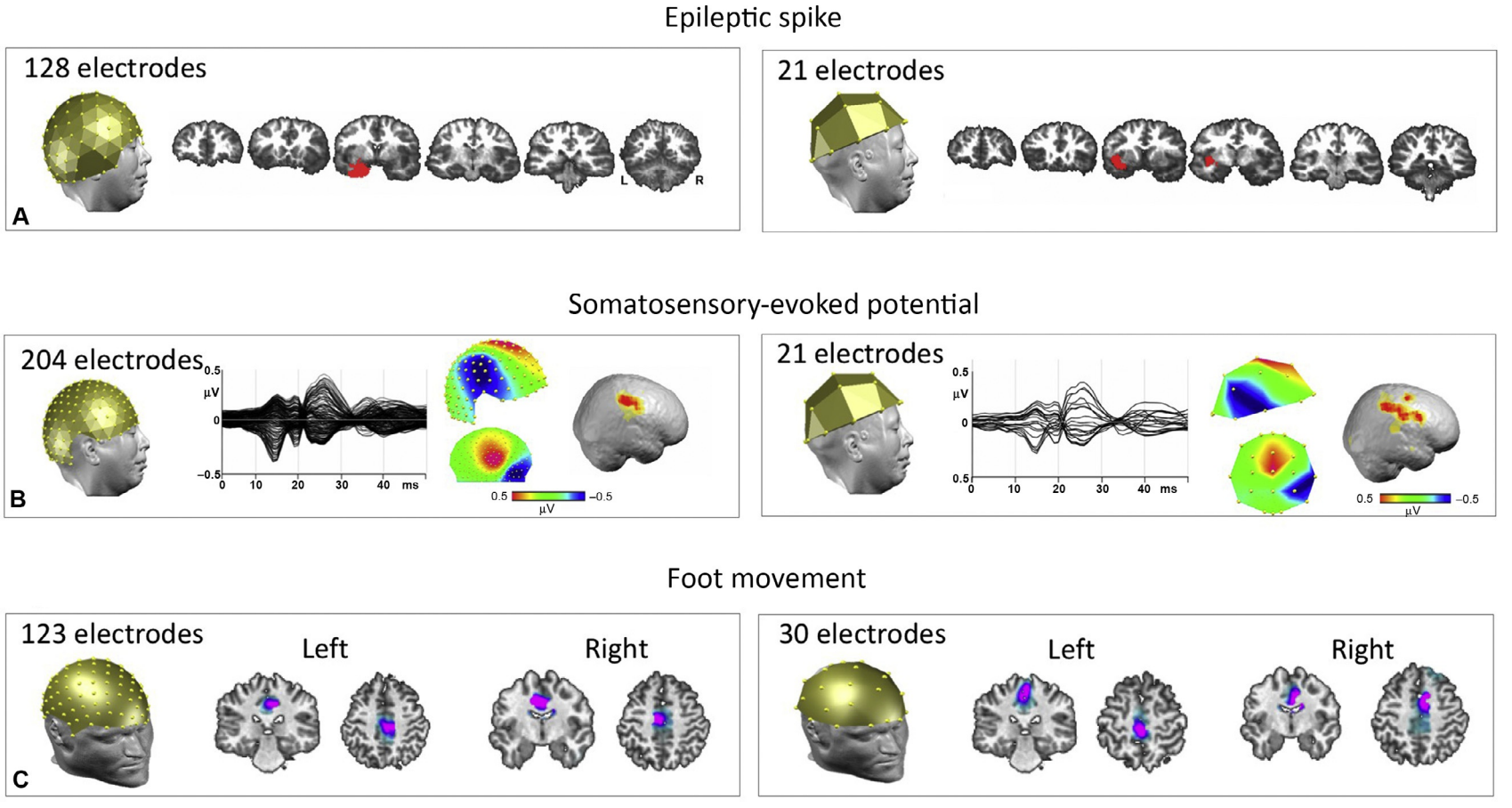

Fig. 12.7. Examples of incorrect source localization with low-resolution EEG. Three examples of source localization using a linear distributed inverse solution are shown for EEG recorded with high resolution and subsequently downsampled to fewer electrodes. (A) Localization of an averaged spike in a patient with temporal lobe epilepsy. The 128-channel recording shows correct localization in the inferior temporal lobe, while a 21-channel recording using the 12–20 system (see Fig. 12.6) misplaces the source on the level of the insula. (B). Somatosensory evoked potential after left thumb air-puff stimulation of a subject recorded with 204 electrodes, correctly identifying the somatosensory cortex. Downsampling to 21 electrodes leads to a blurred distribution of the activity. (C). Localization of high beta (28–30 Hz) amplitude changes during averaged brisk right and left foot movements in a subject recorded with 123 electrodes. Source reconstruction using the individual MRI as head model leads to distinct contralateral beta-decrease relative to a premovement reference period. The same analysis using only 30 out of the 123 electrodes leads to wrong (ipsilateral) localization. Panel (A): Modified from Sperli F, Spinelli L, Seeck M et al. (2006). EEG source imaging in paediatric epilepsy surgery: a new perspective in presurgical workup. Epilepsia 47: 981–990. Panel (B): From Michel CM, Koenig T, Brandeis D et al. (eds.) (2009). Electrical neuroimaging. Cambridge: Cambridge University Press. Panel (C): Courtesy: Dr. Martin Seeber.

positive and negative potentials over the whole head. Depending on the location and the orientation of the equivalent dipoles, the maxima and minima of the potential field can be located at or beyond the border of the conventional electrode arrays, for example, at the level of the mastoids or the cheeks. If these parts of the field are not captured, the estimation of the generators in the brain is not possible. Both extremes of the field should lie within the array to properly recover the gradients and the current density of the field. This fact is particularly important for tangential sources because the maximum and minimum of the generating field do not lie above the source. The effect of bad sampling on source estimation is shown with different examples in Fig. 12.7, including localization of an epileptic focus in the mesial temporal lobe: when the electrodes on the lower part of the temporal lobe are not considered in the source localization reconstruction, the focus is incorrectly localized on the level of the insula rather than the inferior temporal lobe. In fact, mesial temporal sources are systematically misplaced with the conventional 10–20 system, which does not include inferior temporal electrodes, as shown in Sperli et al. (2006).

CONCLUSION

This chapter discusses the history and the development of analyses for high-resolution EEG. It illustrates the additional information that can be gained using high-density electrode arrays and the disadvantages when spatial analyses of electric fields are performed on low-channel counts. It has become clear that the spatial frequency of the scalp electric field is much higher than initially assumed and that incorrect sampling of these frequencies and insufficient coverage of the scalp surface lead to erroneous maps, wrong localization, and failure to detect focal events that are seen by a few electrodes only. Therefore, adequate sampling of the scalp potential field for topographic analysis requires a large number of electrodes.

While this has been a challenge for routine application because of the time needed to apply the electrodes and the hardware required for the collection of such a large amount of data, this is no longer a serious problem. EEG systems of up to 256 electrodes are commercially available. The fast application of electrode caps or nets containing these large numbers of electrodes is now possible, making high-density EEG very feasible in clinical practice (Michel et al., 2004a; Holmes, 2008). Several recent studies showed the possibility and the clinical yield of high-density EEG recordings in the intensive care unit (Boly and Maganti, 2014; Eytan et al., 2016; Chennu et al., 2017), during long-term monitoring for epilepsy (Boly et al., 2017; Nemtsas et al., 2017), as well as during sleep (Lustenberger and Huber, 2012; Siclari et al., 2017).

Given the general recognition of the need and value of high-resolution EEG, it is to be expected that new systems will become available in the near future that make such recordings even easier, faster, more flexible, and more affordable and make the analysis more automatized and standardized. In view of the promising results of EEG source imaging with high-density EEG, particularly in the field of epilepsy, it is evident that this method should and will find its place in the routine workup of patients with focal epilepsy in the foreseeable future (Plummer et al., 2008), as recommended in a recent guideline for presurgical epilepsy evaluation (Rosenow et al., 2016).

However, in addition to the use of high-resolution EEG for source imaging, many new approaches to EEG analysis based on spatial features of the electric field have been developed and successfully applied in clinical and experimental studies. Statistical topographic analyses of EEG and evoked potentials (Murray et al., 2009; Koenig et al., 2014), spatiotemporal decomposition (Spencer et al., 2001; Onton et al., 2006; Michel and Murray, 2012; Michel and Koenig, 2017), and connectivity analyses on the scalp or source level (Astolfi et al., 2004; Nolte et al., 2004; Stam et al., 2007; He et al., 2011a) are methods that rely on the signals measured from multichannel arrays. Their value in understanding the dynamics of large-scale networks of the human brain and as markers for neuropsychiatric diseases has been increasingly demonstrated.

References

Adrian ED, Matthews BHC (1934). The Berger rhythm: potential changes from the occipital lobes in man. Brain 57: 355–385.

Ary JP, Klein SA, Fender DH (1981). Location of sources of evoked scalp potentials: corrections for skull and scalp thicknesses. IEEE Trans Biomed Eng 128: 447–452.

Astolfi L, Cincotti F, Mattia D et al. (2004). Estimation of the effective and functional human cortical connectivity with structural equation modeling and directed transfer function applied to high-resolution EEG. Magn Reson Imaging 22: 1457–1470.

Basar E, Demiralp T, Schurmann M et al. (1999). Oscillatory brain dynamics, wavelet analysis, and cognition. Brain Lang 66: 146–183.

Benar C, Aghakhani Y, Wang Y et al. (2003). Quality of EEG in simultaneous EEG-fMRI for epilepsy. Clin Neurophysiol 114: 569–580.

Bertrand O, Bohorquez J, Pernier J (1994). Time-frequency digital filtering based on an invertible wavelet transform: an application to evoked potentials. IEEE Trans Biomed Eng 41: 77–88.

Birot G, Spinelli L, Vulliemoz S et al. (2014). Head model and electrical source imaging: a study of 38 epileptic patients. Neuroimage Clin 5: 77–83.

Boly M, Maganti R (2014). Monitoring epilepsy in the intensive care unit: current state of facts and potential interest of high density EEG. Brain Inj 28: 1151–1155.

Boly M, Jones B, Findlay G et al. (2017). Altered sleep homeostasis correlates with cognitive impairment in patients with focal epilepsy. Brain 140: 1026–1040.

Bosch-Bayard J, Valdes-Sosa P, Virues-Alba T et al. (2001). 3D statistical parametric mapping of EEG source spectra by means of variable resolution electromagnetic tomography (VARETA). Clin Electroencephalogr 32: 47–61.

Brandeis D, Lehmann D (1986). Event-related potentials of the brain and cognitive processes: approaches and applications. Neuropsychologia 24: 151–168.

Brandeis D, Naylor H, Halliday R et al. (1992). Scopolamine effects on visual information processing, attention, and event-related potential map latencies. Psychophysiology 29: 315–336.

Brodbeck V, Spinelli L, Lascano AM et al. (2011). Electroencephalographic source imaging: a prospective study of 152 operated epileptic patients. Brain 134: 2887–2897.

Brunet D, Murray MM, Michel CM (2011). Spatiotemporal analysis of multichannel EEG: CARTOOL. Comput Intell Neurosci 2011: 813870.

Chella F, Pizzella V, Zappasodi F et al. (2016). Impact of the reference choice on scalp EEG connectivity estimation. J Neural Eng 13:036016.

Chella F, D'andrea A, Basti A et al. (2017). Non-linear analysis of scalp EEG by using bispectra: the effect of the reference choice. Front Neurosci 11: 262.

Chennu S, Annen J, Wannez S et al. (2017). Brain networks predict metabolism, diagnosis and prognosis at the bedside in disorders of consciousness. Brain 140: 2120–2132.

Cooper R, Winther AL, Crow HJ et al. (1965). Comparison of subcortical, cortical and scalp activity using chronically indwelling electrodes in man. Electroencephalogr Clin Neurophysiol 18: 217–228.

Custo A, Van De Ville D, Wells WM et al. (2017). Electroencephalographic Resting-State Networks: broadband resting state topographies' source localization. Brain Connect 7 (10): 671–682.

Darcey TM, Williamson PD (1985). Spatio-temporal EEG measures and their application to human intracranially recorded epileptic seizures. Electroencephalogr Clin Neurophysiol 61: 573–587.

Debener S, Mullinger KJ, Niazy RK et al. (2008). Properties of the ballistocardiogram artefact as revealed by EEG recordings at 1.5, 3 and 7 T static magnetic field strength. Int J Psychophysiol 67: 189–199.

Di Russo F, Pitzalis S, Spitoni G et al. (2005). Identification of the neural sources of the pattern-reversal VEP. Neuroimage 24: 874–886.

Dien J, Beal DJ, Berg P (2005). Optimizing principal components analysis of event-related potentials: matrix type, factor loading weighting, extraction, and rotations. Clin Neurophysiol 116: 1808–1825.

Duffy FH (1985). The BEAM method for neurophysiological diagnosis. Ann N Y Acad Sci 457: 19–34.

Duffy FH (Ed.), (1986). Topographic Mapping of brain electrical activity, Butterworth, Boston.

Duffy FH, Hughes JR, Miranda F et al. (1994). Status of quantitative EEG (QEEG) in clinical practice, 1994. Clin Electroencephalogr 25: VI–XXII.

Eytan D, Pang EW, Doesburg SM et al. (2016). Bedside functional brain imaging in critically-ill children using high-density EEG source modeling and multi-modal sensory stimulation. Neuroimage Clin 12: 198–211.

Fender D, Gevins AS (1987). Source localization of brain electrical activity. In: A Remond (Ed.), Methods of analysis of brain electrical and magnetic signals, Elsevier Science Publishers, Amsterdam.

Fifer WP, Grieve PG, Grose-Fifer J et al. (2006). High-density electroencephalogram monitoring in the neonate. Clin Perinatol 33: 679–691. vii.

Freeman WJ, Holmes MD, Burke BC et al. (2003). Spatial spectra of scalp EEG and EMG from awake humans. Clin Neurophysiol 114: 1053–1068.

Geisler CD, Gerstein GL (1961). The surface EEG in relation to its sources. Electroencephalogr Clin Neurophysiol 13: 927–934.

Geselowitz DB (1998). The zero of potential. IEEE Eng Med Biol Mag 17: 128–132.

Gevins A, Brickett P, Costales B et al. (1990). Beyond topographic mapping: towards functional-anatomical imaging with 124-channel EEGs and 3-D MRIs. Brain Topogr 3: 53–64.

Gorodnitsky IF, George JS, Rao BD (1995). Neuromagnetic source imaging with FOCUSS: a recursive weighted minimum norm algorithm. Electroencephalogr Clin Neurophysiol 95: 231–251.

Grave de Peralta Menendez R, Murray MM, Michel CM et al. (2004). Electrical neuroimaging based on biophysical constraints. Neuroimage 21: 527–539.

Grieve PG, Emerson RG, Isler JR et al. (2004). Quantitative analysis of spatial sampling error in the infant and adult electroencephalogram. Neuroimage 21: 1260–1274.

Hagemann D, Naumann E, Thayer JF (2001). The quest for the EEG reference revisited: a glance from brain asymmetry research. Psychophysiology 38: 847–857.

Hämäläinen MS, Ilmoniemi RJ (1984). Interpreting measured magnetic fields of the brain: estimation of current distributions, Helsinki University of Technology, Helsinki.

Hämälainen MS, Hari R, Ilmoniemi RJ et al. (1993). Magnetoencephalography—theory, instrumentation, and applications to noninvasive studies of the working human brain. Rev Mod Phys 65: 413–497.

Harner R (1988). Brain mapping or spatial analysis? Brain Topogr 1: 73–75.

He B, Ding L (2013). Electrophysiological neuroimaging. In: B He (Ed.), Neural engineering, Springer, New York.

He B, Lian J (2002). High-resolution spatio-temporal functional neuroimaging of brain activity. Crit Rev Biomed Eng 30: 283–306.

He B, Lian J, He B (2005). Electrophysiological neuroimaging: solving the EEG inverse problem. In: Neural engineering, Kluwer Academic Publishers, Norwell, USA.

He B, Dai Y, Astolfi L et al. (2011a). eConnectome: a MATLAB toolbox for mapping and imaging of brain functional connectivity. J Neurosci Methods 195: 261–269.

He B, Yang L, Wilke C et al. (2011b). Electrophysiological imaging of brain activity and connectivity—challenges and opportunities. IEEE Trans Biomed Eng 58: 1918–1931.

Helmholtz HLP (1853). Ueber einige gesetze der vertheilung elektrischer ströme in körperlichen leitern mit anwendung aud die thierisch-elektrischen versuche. Ann Phys Chem 9: 211–233.

Hoekema R, Wieneke GH, Leijten FS et al. (2003). Measurement of the conductivity of skull, temporarily removed during epilepsy surgery. Brain Topogr 16: 29–38.

Holmes MD (2008). Dense array EEG: methodology and new hypothesis on epilepsy syndromes. Epilepsia 49: 3–14.

Hyvarinen A, Oja E (2000). Independent component analysis: algorithms and applications. Neural Netw 13: 411–430.

Jasper H (1958). The ten ± twenty electrode system of the International Federation. Electroencephalogr Clin Neurophysiol Suppl 10: 371–375.

John ER, Karmel BZ, Corning WC et al. (1977). Neurometrics. Science 196: 1393–1410.

Jung TP, Makeig S, Humphries C et al. (2000). Removing electroencephalographic artifacts by blind source separation. Psychophysiology 37: 163–178.

Jung TP, Makeig S, Mckeown MJ et al. (2001). Imaging brain dynamics using independent component analysis. Proc IEEE 89: 1107–1112.

Kayser J, Tenke CE (2005). Trusting in or breaking with convention: towards a renaissance of principal components analysis in electrophysiology. Clin Neurophysiol 116: 1747–1753.

Khanna A, Pascual-Leone A, Michel CM et al. (2015). Microstates in resting-state EEG: current status and future directions. Neurosci Biobehav Rev 49: 105–113.

Klamer S, Elshahabi A, Lerche H et al. (2015). Differences between MEG and high-density EEG source localizations using a distributed source model in comparison to fMRI. Brain Topogr 28: 87–94.

Koenig T, Melie-Garcia L (2010). A method to determine the presence of averaged event-related fields using randomization tests. Brain Topogr 23: 233–242.

Koenig T, Studer D, Hubl D et al. (2005). Brain connectivity at different time-scales measured with EEG. Philos Trans R Soc Lond B Biol Sci 360: 1015–1023.

Koenig T, Stein M, Grieder M et al. (2014). A tutorial on data-driven methods for statistically assessing ERP topographies. Brain Topogr 27: 72–83.

Koles ZJ, Lind JC, Soong AC (1995). Spatio-temporal decomposition of the EEG: a general approach to the isolation and localization of sources. Electroencephalogr Clin Neurophysiol 95: 219–230.

Kuhnke N, Schwind J, Dümpelmann M et al. (2018). High frequency oscillations in the ripple band (80–250 Hz) in scalp EEG: higher density of electrodes allows for better localization of the seizure onset zone. Brain Topogr 31 (6): 1059–1072.

Lai Y, Van Drongelen W, Ding L et al. (2005). Estimation of in vivo human brain-to-skull conductivity ratio from simultaneous extra- and intra-cranial electrical potential recordings. Clin Neurophysiol 116: 456–465.

Lantz G, Grave De Peralta R, Spinelli L et al. (2003). Epileptic source localization with high density EEG: how many electrodes are needed. Clin Neurophysiol 114: 63–69.

Lascano AM, Grouiller F, Genetti M et al. (2014). Surgically relevant localization of the central sulcus with high-density somatosensory-evoked potentials compared with functional magnetic resonance imaging. Neurosurgery 74: 517–526.

Lehmann D (1987). Principles of spatial analysis. In: AS Gevins, A Remont (Eds.), Methods of analysis of brain electrical and magnetic signals, Elsevier, Amsterdam.

Lehmann D (1990). Brain electric microstates and cognition: the atoms of thought. In: ER John (Ed.), Machinery of the mind, Birkhäuser, Boston.

Lehmann D, Michel CM (2011). EEG-defined functional microstates as basic building blocks of mental processes. Clin Neurophysiol 122: 1073–1074.

Lehmann D, Skrandies W (1980). Reference-free identification of components of checkerboard-evoked multichannel potential fields. Electroencephalogr Clin Neurophysiol 48: 609–621.

Lehmann D, Kavanagh RH, Fender DH (1969). Field studies of averaged visually evoked EEG potentials in a patient with a split chiasm. Electroencephalogr Clin Neurophysiol 26: 193–199.

Lehmann D, Ozaki H, Pal I (1986). Averaging of spectral power and phase via vector diagram best fits without reference electrode or reference channel. Electroencephalogr Clin Neurophysiol 64: 350–363.

Lehmann D, Ozaki H, Pal I (1987). EEG alpha map series: brain micro-states by space-oriented adaptive segmentation. Electroencephalogr Clin Neurophysiol 67: 271–288.

Lehmann D, Pascual-Marqui R, Michel CM (2009). EEG microstates. Scholarpedia 4: 7632.

Li T-H, North G (1996). Aliasing effects and sampling theorems of SRFs when sampled on a finite grid. Ann Inst Stat Math 49: 341–354.

Lopes da Silva FH, Mars NJI (1987). Parametric methods in EEG analysis. In: AS Gevins, A Rémond (Eds.), Methods of analysis of brain electrical and magnetic signals. Handbook of electroencephalography and clinical neurophysiology, Elsevier, Amsterdam.

Lu Y, Worrell GA, Zhang HC et al. (2014). Noninvasive imaging of the high frequency brain activity in focal epilepsy patients. IEEE Trans Biomed Eng 61: 1660–1667.

Lustenberger C, Huber R (2012). High density electroencephalography in sleep research: potential, problems, future perspective. Front Neurol 3: 77.

Luu P, Tucker DM, Englander R et al. (2001). Localizing acute stroke-related EEG changes: assessing the effects of spatial undersampling. J Clin Neurophysiol 18: 302–317.

Makeig S, Jung TP, Bell AJ et al. (1997). Blind separation of auditory event-related brain responses into independent components. Proc Natl Acad Sci USA 94 (10): 979–984.

Makeig S, Westerfield M, Townsend J et al. (1999). Functionally independent components of early event-related potentials in a visual spatial attention task. Philos Trans R Soc Lond B Biol Sci 354: 1135–1144.

Malmivuo JA, Suihko VE (2004). Effect of skull resistivity on the spatial resolutions of EEG and MEG. IEEE Trans Biomed Eng 51: 1276–1280.

Mantini D, Perrucci MG, Cugini S et al. (2007). Complete artifact removal for EEG recorded during continuous fMRI using independent component analysis. Neuroimage 34: 598–607.

Maurer K (1989). Topographic brain mapping of EEG and evoked potentials, Springer Verlag, Berlin.

Megevand P, Spinelli L, Genetti M et al. (2014). Electric source imaging of interictal activity accurately localises the seizure onset zone. J Neurol Neurosurg Psychiatry 85: 38–43.

Michel CM, He B (2018). EEG mapping and source imaging. In: D Schomer, FH Lopes DA Silva (Eds.), Niedermeyer's Electroencephalography. Oxford University Press, New York, pp. 1135–1156.

Michel CM, Koenig T (2017). EEG microstates as a tool to study temporal dynamics of whole-brain neuronal networks. Neuroimage 180: 577–593.

Michel CM, Murray MM (2012). Towards the utilization of EEG as a brain imaging tool. Neuroimage 61: 371–385.

Michel CM, Henggeler B, Lehmann D (1992). 42-channel potential map series to visual contrast and stereo stimuli: perceptual and cognitive event-related segments. Int J Psychophysiol 12: 133–145.

Michel CM, Brandeis D, Skrandies W et al. (1993). Global field power: a 'time-honoured' index for EEG/EP map analysis. Int J Psychophysiol 15: 1–5.

Michel CM, Lantz G, Spinelli L et al. (2004a). 128-channel EEG source imaging in epilepsy: clinical yield and localization precision. J Clin Neurophysiol 21: 71–83.

Michel CM, Murray MM, Lantz G et al. (2004b). EEG source imaging. Clin Neurophysiol 115: 2195–2222.

Michel CM, Koenig T, Brandeis D, Gianotti LRR, Wackermann J (Eds.), (2009). Electrical neuroimaging, Cambridge University Press, Cambridge.

Mosher JC, Lewis PS, Leahy RM (1992). Multiple dipole modeling and localization from spatio-temporal MEG data. IEEE Trans Biomed Eng 39: 541–557.

Murray MM, Brunet D, Michel CM (2008). Topographic ERP analyses: a step-by-step tutorial review. Brain Topogr 20: 249–264.

Murray MM, De Lucia M, Brunet D et al. (2009). Principles of topographic analyses for electrical neuroimaging. In: TC Handy (Ed.), Brain signal analysis, The MIT Press, Cambridge, MA.

Nakamura W, Anami K, Mori T et al. (2006). Removal of ballistocardiogram artifacts from simultaneously recorded EEG and fMRI data using independent component analysis. IEEE Trans Biomed Eng 53: 1294–1308.

Nemtsas P, Birot G, Pittau F et al. (2017). Source localization of ictal epileptic activity based on high-density scalp EEG data. Epilepsia 58: 1027–1036.

Nolte G, Bai O, Wheaton L et al. (2004). Identifying true brain interaction from EEG data using the imaginary part of coherency. Clin Neurophysiol 115: 2292–2307.

Nunez PL (1981). Electric fields of the brain: the neurophysics of EEG, Oxford University Press, New York.

Nuwer MR (1990). On the controversies about clinical use of EEG brain mapping. Brain Topogr 3: 103–111.

Nuwer M (1997). Assessment of digital EEG, quantitative EEG, and EEG brain mapping: report of the American Academy of Neurology and the American Clinical Neurophysiology Society. Neurology 49: 277–292.

Odabaee M, Freeman WJ, Colditz PB et al. (2013). Spatial patterning of the neonatal EEG suggests a need for a high number of electrodes. Neuroimage 68: 229–235.

Odabaee M, Tokariev A, Layeghy S et al. (2014). Neonatal EEG at scalp is focal and implies high skull conductivity in realistic neonatal head models. Neuroimage 96: 73–80.

Onton J, Westerfield M, Townsend J et al. (2006). Imaging human EEG dynamics using independent component analysis. Neurosci Biobehav Rev 30: 808–822.

Oostendorp TF, Delbeke J, Stegeman DF (2000). The conductivity of the human skull: results of in vivo and in vitro measurements. IEEE Trans Biomed Eng 47: 1487–1492.

Pascual-Marqui RD (2002). Standardized low-resolution brain electromagnetic tomography (sLORETA): technical details. Methods Find Exp Clin Pharmacol 24: 5–12.

Pascual-Marqui RD, Lehmann D (1993). Topographic maps, source localization inference, and the reference electrode: comments on a paper by Desmedt et al. Electroencephalogr Clin Neurophysiol 88: 532–536.

Pascual-Marqui RD, Michel CM, Lehmann D (1994). Low resolution electromagnetic tomography: a new method for localizing electrical activity in the brain. Int J Psychophysiol 18: 49–65.

Pascual-Marqui RD, Michel CM, Lehmann D (1995). Segmentation of brain electrical activity into microstates: model estimation and validation. IEEE Trans Biomed Eng 42: 658–665.

Pascual-Marqui RD, Sekihara K, Brandeis D et al. (2009). Imaging the electrical neuronal generators of EEG/MEG. In: CM Michel, T Koenig, D Brandeis, LRR Gianotti, J Wackermann (Eds.), Electrical neuroimaging. Cambridge University Press, Cambridge.

Petrov Y, Nador J, Hughes C et al. (2014). Ultra-dense EEG sampling results in two-fold increase of functional brain information. Neuroimage 90: 140–145.

Picton TW, Alain C, Woods DL et al. (1999). Intracerebral sources of human auditory-evoked potentials. Audiol Neurootol 4: 64–79.

Plummer C, Harvey AS, Cook M (2008). EEG source localization in focal epilepsy: where are we now? Epilepsia 49: 201–218.

Pourtois G, Deplanque S, Christoph M et al. (2008). Beyond the conventional event-related brain potential (ERP): exploring the time-course of visual emotion processing using topographic and principal component analyses. Brain Topogr 20: 265–277.

Ragot RA, Remond A (1978). EEG field mapping. Electroencephalogr Clin Neurophysiol 45: 417–421.

Rieger K, Diaz Hernandez L, Baenninger A et al. (2016). 15 Years of microstate research in schizophrenia—where are we? A meta-analysis. Front Psych 7: 22.

Rose S, Ebersole JS (2009). Advances in spike localization with EEG dipole modeling. Clin EEG Neurosci 40: 281–287.

Rosenow F, Bast T, Czech T et al. (2016). Revised version of quality guidelines for presurgical epilepsy evaluation and surgical epilepsy therapy issued by the Austrian, German, and Swiss working group on presurgical epilepsy diagnosis and operative epilepsy treatment. Epilepsia 57: 1215–1220.

Rush S, Driscoll DA (1969). EEG electrode sensitivity—an application of reciprocity. IEEE Trans Biomed Eng 16: 15–22.

Ryynanen OR, Hyttinen JA, Laarne PH et al. (2004). Effect of electrode density and measurement noise on the spatial resolution of cortical potential distribution. IEEE Trans Biomed Eng 51: 1547–1554.

Ryynanen OR, Hyttinen JA, Malmivuo JA (2006). Effect of measurement noise and electrode density on the spatial resolution of cortical potential distribution with different resistivity values for the skull. IEEE Trans Biomed Eng 53: 1851–1858.

Salmelin R, Baillet S (2009). Electromagnetic brain imaging. Hum Brain Mapp 30: 1753–1757.

Sanei S, Chambers J (2007). EEG source localization. In: S Sanei, J Chambers (Eds.), EEG signal processing, John Wiley and Sons, Ltd, New Jersey.

Scherg M, Ebersole JS (1994). Brain source imaging of focal and multifocal epileptiform EEG activity. Neurophysiol Clin 24: 51–60.

Scherg M, Picton TW (1991). Separation and identification of event-related potential components by brain electric source analysis. In: CHM Brunia, G Mulder, MN Verbaten (Eds.), Event-related brain research, Elsevier, Amsterdam.

Scherg M, von Cramon D (1985). A new interpretation of the generators of BAEP waves I-V: results of a spatio-temporal dipole model. Electroencephalogr Clin Neurophysiol 62: 290–299.

Scherg M, Vajsar J, Picton TW (1989). A source analysis of the late human auditory evoked potential. J Cogn Neurosci 1: 336–355.

Sekihara K, Nagarajan SS, Poeppel D et al. (2001). Reconstructing spatio-temporal activities of neural sources using an MEG vector beamformer technique. IEEE Trans Biomed Eng 48: 760–771.

Siclari F, Baird B, Perogamvros L et al. (2017). The neural correlates of dreaming. Nat Neurosci 20: 872–878.

Skrandies W (1989). Data reduction of multichannel fields: global field power and principal component analysis. Brain Topogr 2: 73–80.

Skrandies W (1990). Global field power and topographic similarity. Brain Topogr 3: 137–141.

Skrandies W (1993). EEG/EP: new techniques. Brain Topogr 5: 347–350.

Sohrabpour A, Lu Y, Kankirawatana P et al. (2015). Effect of EEG electrode number on epileptic source localization in pediatric patients. Clin Neurophysiol 126: 472–480.

Spencer KM, Dien J, Donchin E (2001). Spatiotemporal analysis of the late ERP responses to deviant stimuli. Psychophysiology 38: 343–358.

Sperli F, Spinelli L, Seeck M et al. (2006). EEG source imaging in paediatric epilepsy surgery: a new perspective in presurgical workup. Epilepsia 47: 981–990.

Spitzer AR, Cohen LG, Fabrikant J et al. (1989). A method for determining optimal interelectrode spacing for cerebral topographic mapping. Electroencephalogr Clin Neurophysiol 72: 355–361.

Srinivasan R, Nunez PL, Tucker DM et al. (1996). Spatial sampling and filtering of EEG with spline Laplacians to estimate cortical potentials. Brain Topogr 8: 355–366.

Srinivasan R, Tucker DM, Murias M (1998). Estimating the spatial Nyquist of the human EEG. Behav Res Methods Instrum Comput 30: 8–19.

Stam CJ, Nolte G, Daffertshofer A (2007). Phase lag index: assessment of functional connectivity from multi channel EEG and MEG with diminished bias from common sources. Hum Brain Mapp 28: 1178–1193.

Tang C, You F, Cheng G et al. (2008). Correlation between structure and resistivity variations of the live human skull. IEEE Trans Biomed Eng 55: 2286–2292.

Vaughan HGJ (1982). The neural origins of human event-related potentials. Ann N Y Acad Sci 388: 125–138.

Waberski TD, Lamberty K, Dieckhofer A et al. (2008). Short-term modulation of the ipsilateral primary sensory cortex by nociceptive interference revealed by SEPs. Neurosci Lett 435: 137–141.

Womelsdorf T, Schoffelen JM, Oostenveld R et al. (2007). Modulation of neuronal interactions through neuronal synchronization. Science 316: 1609–1612.

Wong P (1990). Introduction to brain topography, Plenum Press, New York.

Zelmann R, Lina JM, Schulze-Bonhage A et al. (2014). Scalp EEG is not a blur: it can see high frequency oscillations although their generators are small. Brain Topogr 27: 683–704.